Coherence of phonon avalanches in ruby

L. G. Tilstra, A. F. M. Arts, and H. W. de Wijn*

Faculty of Physics and Astronomy, and Debye Institute, Utrecht University, P.O. Box 80000, 3508 TA Utrecht, The Netherlands

(Received 9 June 2003; published 20 October 2003)

Phonon avalanches resonant with the optically inverted Zeeman-split $\bar{E}(^2E)$ doublet of Cr^{3+} have been measured and analyzed in a single crystal of 500-at. ppm ruby ($Al_2O_3:Cr^{3+}$) with a geometry adapted to the study of coherence. A set of coherent Bloch equations governing the interacting acoustic wave and spin polarizations is found to provide an excellent description of the results, and to be far superior to incoherent rate equations for the phonon and level populations. The dephasing time conforms with the width of the inhomogeneously broadened transition connecting the $\bar{E}(^2E)$ states, which indicates that dephasing primarily occurs by the spread in frequencies.

DOI: 10.1103/PhysRevB.68.144302 PACS number(s): 63.20.−e

I. INTRODUCTION

This paper is concerned with coherence of the phonon avalanches released by dilute centers in crystalline media, more specifically by the one-phonon transition connecting the optically excited Zeeman-split $\bar{E}(^2E)$ doublet states in dilute ruby ($Al_2O_3:Cr^{3+}$). Phonon avalanches result from stimulated emission of phonons following population inversion of the participating levels, which are often referred to as the spin system. They entail a rapid heating, i.e., an intense increase in the occupations, of the phonon modes that are "on speaking terms" with the spins, and accordingly manifest themselves through an enhanced spin-lattice relaxation. For this to occur, however, the energy that the inverted spin system stores into the resonant lattice vibrations must exceed the energy the latter lose by relaxation, so that the phonon occupations are driven out of thermal equilibrium. This condition is called phonon bottleneck.

Phonon avalanches were first observed by Brya and Wagner[1] using microwave techniques in dilute cerium lanthanum magnesium nitrate. These authors relied on a set of rate equations for the populations of the phonon modes and the spin levels to successfully describe their observations. The $\bar{E}(^2E)$ doublet in dilute ruby has in the mean time become an archetypal system for the observation of phonon avalanches,[2–5] because complete initial population inversion of the doublet is feasible by selective optical pumping, Kramers symmetry ensures the transition to be narrow, the frequency and spin-lattice relaxation time may be varied over wide ranges, and luminescent techniques enable sensitive phonon detection. Other systems in which phonon avalanches were observed include $Al_2O_3:V^{4+}$,[6] the $2\bar{A}(^2E)$-$\bar{E}(^2E)$ transition in ruby at 29 cm^{-1},[7] $LaF_3:Er^{3+}$,[8] and the $^4A_2$ ground state in ruby at 9.1 GHz.[9] The data could usually be described on the basis of rate equations, which provide a by nature incoherent description, yet a sizable degree of coherence was later inferred in the spin-phonon interaction of dilute cerium lanthanum magnesium nitrate.[10]

The problem of coherence of phonon avalanches has indeed been quite elusive, mainly because the detection techniques for phonons are quite indirect. With luminescent detection, as a case in point, the generation of phonons is felt by a changing optical intensity measuring the population of a suitable spin level. Another point of concern is to avoid the complications associated with an extended volume, such as travel of the phonons beyond the inverted zone,[3,5] the finite penetration depth of the laser light, and inhomogeneity in the $\bar{E}(^2E)$ splitting by the external magnetic field. In the present study, the experimental conditions are adapted to the problem at issue by the use of a specimen so thin that (i) uniform laser illumination is ensured, and (ii) the phonons cover the distance between the crystal faces well within the time the avalanche requires to develop.

In Sec. II, we introduce the $\bar{E}(^2E)$ level system and the frequently used but, as we will verify in Sec. V, deficient description of the avalanche in terms of rate equations for the phonon and spin populations. In Sec. IV, we derive a set of coherent Bloch equations, which are more complete in that they include the transverse components of the spins and the acoustic waves. Finally, in Sec. V, we see that the Bloch equations describe the experiments conducted in Sec. III for a series of initial inversions in a way that is significant from the point of view of the physics.

II. LEVEL SCHEME AND RATE EQUATIONS

The relevant energy levels of Cr^{3+} in Al_2O_3 are shown in Fig. 1. One of the merits of this level system is the metastable $\bar{E}(^2E)$ doublet, whose states, when split by an external magnetic field, are connected by a one-phonon transition. Orbach and Raman relaxation processes are completely frozen out at the cryogenic temperatures used.[11] The upper level of $\bar{E}(^2E)$ may furthermore be preferentially populated by selective pulsed optical pumping. For the study of stimulated phonon emission, therefore, the $\bar{E}(^2E)$ doublet is ideally suited, more so because the development of the phonon avalanche may be monitored through the growing population of the lower level and the ensuing luminescent return to $^4A_2$ (cf. Fig. 1). Other advantages are the small bandwidth of the phonon transition, and the wide range of values, attainable via adjustment of the external magnetic field $\mathbf{B}$, for the $\bar{E}(^2E)$ level splitting and the spin-lattice relaxation. For the highly anisotropic Zeeman splitting we have $\hbar\omega = \mu_B B[(g_\parallel \cos\vartheta)^2 + (g_\perp \sin\vartheta)^2]^{1/2}$, in which ϑ is the angle

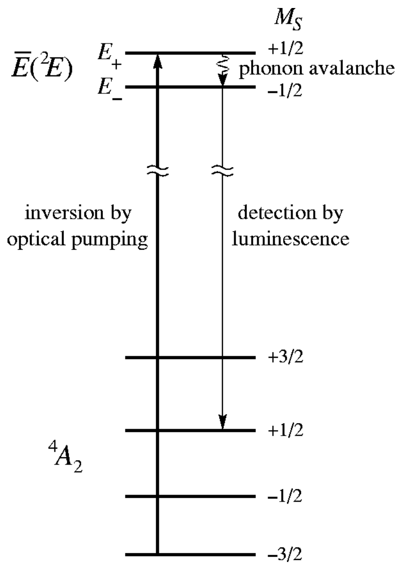

FIG. 1. The $\bar{E}(^2E)$ metastable doublet and the $^4A_2$ ground quartet of Cr^{3+} in ruby split up in an external magnetic field. Following selective pulsed optical excitation, the $\bar{E}(^2E)$ two-level system is fully inverted. Subsequently, a phonon avalanche develops, which is detected via the luminescence. The Zeeman splittings are drawn to scale for the field used ($B=3.48$ T at $\vartheta=65°$). The $\bar{E}(^2E)$ states are split by 1.68 cm^{-1}. The $\bar{E}(^2E)$-$^4A_2$ separation is 14 430 cm^{-1}.

the field makes with the c axis, $g_\parallel=2.445$,[12] and $g_\perp=0.0515$.[13,14] The spin-lattice relaxation time T_1 within $\bar{E}(^2E)$ strongly depends on the magnetic field. It is given by $T_1^{-1}=CB^5\sin^2\vartheta\cos^3\vartheta$ from theory,[15] with $C=47\ \mathrm{T}^{-5}\ \mathrm{s}^{-1}$ from experiment.[16] The lattice furthermore is little anharmonic, so that dilute ruby shows only weak phonon losses at cryogenic temperatures.[17]

A simple description of the phonon avalanche developing after complete population inversion of $\bar{E}(^2E)$ is provided by incoherent rate equations governing the population densities N_+ and N_- of the $\bar{E}(^2E)$ levels on the one hand and the occupation number p per unit of volume of the resonant phonon modes on the other.[3] The equations, which despite their shortcomings provide a substantial level of understanding of phonon avalanches, read

$$\frac{dp}{dt}=\frac{(p+1)N_+-pN_-}{\rho\Delta\nu T_1}-\frac{p-p_0}{\tau_{\mathrm{ph}}}, \tag{1}$$

$$\frac{dN_+}{dt}=-\frac{(p+1)N_+-pN_-}{T_1}-\frac{N_+}{\tau_R}, \tag{2}$$

$$\frac{dN_-}{dt}=\frac{(p+1)N_+-pN_-}{T_1}-\frac{N_-}{\tau_R}. \tag{3}$$

The first terms on the right-hand side describe spontaneous emission, stimulated emission, and absorption of phonons resonant with the $\bar{E}(^2E)$ states. The quantity ρ denotes the density of phonon modes per unit of frequency, so that $\rho\Delta\nu$, with $\Delta\nu$ being the full bandwidth of the $E_+\leftrightarrow E_-$ transition, is the density of resonant phonon modes. Notice that, for simplicity, p is taken uniform over these modes, and that the spin-lattice relaxation time T_1, which represents the spin-phonon coupling, refers to relaxation of the spins. The remaining terms represent the radiative decay of $\bar{E}(^2E)$ back to the $^4A_2$ ground multiplet with time constant $\tau_R\approx5$ ms, somewhat dependent on the conditions, and phonon losses with time constant τ_{ph}, at this point without concern about the exact nature of these losses. We further define $N^*=N_++N_-$ for the momentary density of excited Cr^{3+} centers. For large N^*, more precisely if $N^*\tau_{\mathrm{ph}}/\rho\Delta\nu T_1\gtrsim1$, the generated phonons have insufficient time to decay, so that p will be driven out of its thermal equilibrium value $p_0=1/[\exp(\hbar\omega/k_BT_0)-1]$, with T_0 being the temperature of the lattice. Adding Eqs. (2) and (3), we further see that $N^*(t)=N_0^*e^{-t/\tau_R}$, where N_0^* is the population density of $\bar{E}(^2E)$ just after the laser pulse. Note that N^* decreases by no more than 0.1% in the time span of a phonon avalanche.

III. EXPERIMENTS

The specimen used in the present experiments is a thin cuboidal slab of Czochralski-grown single-crystalline ruby with a Cr^{3+} concentration of 500 at. ppm. It measures $8.2\times1.5\ \mathrm{mm}^2$ in area and is 200 μm thick. The crystalline a axis is at right angles with the main faces, while the c axis is parallel with these faces at an angle of 25° with the longest dimension. The faces were polished to better than 10-nm roughness to reduce undesirable light scattering and phonon loss at the surfaces.

The ruby slab was mounted upright in an optical cryostat equipped with a split-coil superconducting magnet, and immersed in liquid He regulated to $T_0=1.4$ K. The magnetic field, of magnitude $B=3.48$ T, is directed perpendicular to the a axis and the longest crystal dimension, i.e., at $\vartheta=65°$ from the c axis. The $\bar{E}(^2E)$ Zeeman splitting accordingly is $\omega/2\pi c=1.68\ \mathrm{cm}^{-1}$. We further have $T_1=0.67$ ms, sufficiently long to see the avalanche grow, yet short enough to allow thermalization among E_+ and E_- prior to radiative decay.

The optical excitation to E_+ was achieved with a pulsed dye laser, operating with LDS 698 dye and pumped with the 532-nm frequency-doubled output of a Q-switched Nd:YAG (yttrium aluminum garnet) laser. The laser delivered light pulses of 8 ns duration at 50 Hz repetition, and was tuned to a wavelength of 693 nm to excite Cr^{3+} from the $^4A_2$, $M_S=-\frac{3}{2}$ ground state to E_+ (Fig. 1). The laser beam is incident along the a axis, which in ruby is a phonon-focusing direction.[18] Only the center portion of the beam was focused to a waist $\approx200\ \mu$m in diameter. The geometry permits adjustment of the light polarization to any angle ϑ_{pol} with the c axis. The initial $\bar{E}(^2E)$ population density N_0^* appears to depend on ϑ_{pol} according to $1-0.70\cos^2\vartheta_{\mathrm{pol}}$. The polarization was usually chosen along the c axis, despite the reduced efficiency, because this minimizes residual Rayleigh scattering. Control over power and polarization of the laser light was achieved with polarization filters, polarization rotators, and calibrated gray filters.

The phonon avalanches were detected via the growing intensity of a suitable Zeeman component of the $E_- \rightarrow {}^4A_2$ luminescence, as indicated in Fig. 1. The $E_- \rightarrow {}^4A_2$ luminescent spectrum and the initially stronger $E_+ \rightarrow {}^4A_2$ spectrum each consist of four Zeeman transitions. To separate these optimally, the $\bar{E}({}^2E)$ splitting is chosen equal to half the ${}^4A_2$ level spacing, so that the luminescent transitions are about equidistant and depart alternately from E_+ and E_-. The transition intensities were measured versus the time by means of a 0.85-m Czerny-Turner double monochromator followed by a cooled photomultiplier operating in photon-counting mode and a fast multichannel scaler averaging over typically 5000 optical-pumping cycles. The channel dwell time usually was 20 ns.

The intensities of particularly the $E_- \rightarrow {}^4A_2$, $M_S = +\frac{1}{2}$ and $E_+ \rightarrow {}^4A_2$, $M_S = -\frac{1}{2}$ transitions allow us to gauge N_- and N_+, from which, by taking advantage of the Kramers symmetry, the quantity of interest N_-/N_0^* may be derived. Because proper calibration of N_- in terms of N_0^* is important to the analysis in Sec. V below, we have employed two more methods of calibration to find essentially identical results. One of these relies on the Boltzmann equilibrium value N_- reaches after the avalanche has died out. It requires no resetting of the spectrometer to the companion transition departing from E_+, and is insensitive to differences in reabsorption by the various Zeeman states of ${}^4A_2$. In the other method, which is less precise due to statistical noise, N_+ is followed versus the time as it drops from its initial value N_0^*, and N_- is deduced by subtraction.

Figure 2 shows the results for N_-/N_0^* versus the time for a series of laser pulse energies. Not shown is the trace for 22 μJ energy, just above the threshold for avalanches, for which N_- increases significantly only after the time interval displayed. At the lowest energy in Fig. 2, N_- is observed to increase only slowly, but already four times faster than by thermal relaxation alone. Relying for an estimate on the rate Eq. (3), we see that the initial growth of N_- is approximately given by $dN_-/dt \sim (p+1)N_0^*/T_1$, so that $(p+1)/(p_0+1) \sim 4$. With $p_0 = 0.25$, therefore, $p \sim 4$. At the highest laser energy, where the phonon avalanche has fully developed, N_- rises much faster, corresponding to p's on the order of 10^3. Figure 2 only covers the first 5 μs following the laser pulse. At longer times, N_- first reaches thermal equilibrium on a time scale on the order of $T_1/(2p_0+1) = 0.47$ ms, and ultimately decays to zero as a result of the radiative decay of $\bar{E}({}^2E)$ to the ${}^4A_2$ ground multiplet on the even longer time scale $\tau_R \approx 5$ ms.

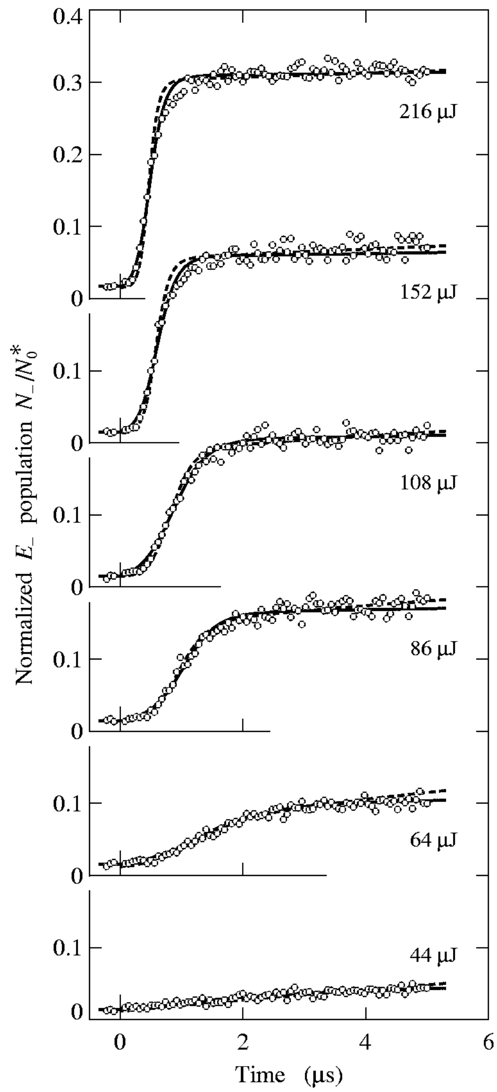

FIG. 2. Growth of N_-, normalized to N_0^*, following pulsed optical pumping into E_+ for a series of laser pulse energies, as indicated. The solid curves are fits of the Bloch Eqs. (15)–(19) to the data. The dashed curves represent fits to the rate Eqs. (1)–(3), yet with an unphysical nonlinear dependence of N_0^* on the pulse energy. For clarity, groups of three successive data points, each with a dwell time of 20 ns, are averaged to a single point in the graphs. The residual N_- at $t=0$ is due to incomplete radiative decay after previous pumping cycles.

IV. BLOCH EQUATIONS

We depart from the Hamiltonian of the coupled lattice-spin system as formulated by Jacobsen and Stevens,[19] which comprises the kinetic and potential lattice energies, the energy of the spin doublets, and finally the interaction of the lattice vibrations with the doublets. That is,

$$\mathcal{H} = \sum_i \left(\frac{\mathcal{P}_i^2}{2M} + \frac{K}{2}(\mathcal{U}_i - \mathcal{U}_{i-1})^2 \right) + \sum_i{}' \hbar\omega \mathcal{S}_i^z + \sum_i{}' \gamma\hbar(\mathcal{U}_{i+1} - \mathcal{U}_{i-1})\mathcal{S}_i^x. \tag{4}$$

The first summation runs over all unit cells, enumerated by i, of a one-dimensional lattice chain, whereas, in keeping with the dilute presence of the spins, the primed summations are restricted to unit cells containing a spin. The quantities $\mathcal{P}_i$ and $\mathcal{U}_i$ denote the momentum and mass-excursion operators of the strain in cell i, while $\mathcal{S}_i^x$ and $\mathcal{S}_i^z$ are the transverse and longitudinal components of the local spin operator. The quantity M is the mass of the unit cell, K is the spring constant between neighboring cells, $\hbar\omega$ stands for the doublet splitting as well as the energy of the resonant phonons, and γ measures the coupling between the strain waves and $\mathcal{S}_i^x$. Note that damping and all other consequences of lattice anharmonicity are ignored.

In a quantum-mechanical treatment, we turn to the Heisenberg picture to derive the time dependence of the operators $\mathcal{P}_i$, $\mathcal{U}_i$, $\mathcal{S}_i^x$, $\mathcal{S}_i^y$, and $\mathcal{S}_i^z$ by the use of $\partial\mathcal{P}_i/\partial t=(i\hbar)^{-1}[\mathcal{P}_i,\mathcal{H}]$, etc. Contracting the resultant expressions by elimination of $\mathcal{P}_i$ and $\mathcal{S}_i^y$, averaging in the quantum-mechanical sense, introducing the abbreviations $U_i=\langle\mathcal{U}_i\rangle$, $S_i^x=\langle\mathcal{S}_i^x\rangle$, and $S_i^z=\langle\mathcal{S}_i^z\rangle$, and finally decoupling the nonlinear combinations $\langle\mathcal{U}_{i\pm1}\mathcal{S}_i^z\rangle$ into the random-phase approximations $U_{i\pm1}S_i^z$, we arrive at

$$\frac{\partial^2 U_i}{\partial t^2}=\frac{K}{M}(U_{i+1}-2U_i+U_{i-1})+\frac{\gamma\hbar}{M}(\epsilon_{i+1}S_{i+1}^x-\epsilon_{i-1}S_{i-1}^x), \tag{5}$$

$$\frac{\partial S_i^z}{\partial t}=-\frac{\gamma}{\omega}(U_{i+1}-U_{i-1})\frac{\partial S_i^x}{\partial t}, \tag{6}$$

$$\left(\frac{\partial^2}{\partial t^2}+\omega^2\right)S_i^x=\gamma\omega(U_{i+1}-U_{i-1})S_i^z, \tag{7}$$

where $\epsilon_i=1$ if unit cell i holds a spin, and $\epsilon_i=0$ otherwise. Equations (6) and (7) are valid only if $\epsilon_i=1$.

To deal with this abundance of coupled equations, we change over, in the customary way, to a continuous acoustic wave $U(x,t)$ such that $U(x,t)$ equals U_i at the successive mass positions. Note that at the present ω the acoustic wavelength amounts to 135 nm, compared to a lattice constant $a\approx0.5$ nm. Similarly, we introduce the continuous spin functions $S^x(x,t)$ and $S^z(x,t)$ matching S_i^x and S_i^z at the spin positions. Continuum approximation of the latter two quantities is allowed, because several tens of excited Cr^{3+} reside within the distance of an acoustic wavelength despite their dilute presence at the typical $N_0^*=10^{23}-10^{24}\ \mathrm{m}^{-3}$.

In the formalism below, we prefer to express the spin excursions in the form of the Bloch vector $(S(x,t),n(x,t))$ defined by

$$S(x,t)=2N^*S^x(x,t), \tag{8}$$

$$n(x,t)=2N^*S^z(x,t), \tag{9}$$

so that $S(x,t)$ represents the transverse polarization of the two-level system, and $n(x,t)$ equals the population difference N_+-N_-, both per unit of volume. Evenly spread over the lattice, a^3N^* spins are thus assigned to each unit cell. The continuous counterparts of Eqs. (5)–(7) then read

$$\frac{\partial^2 U}{\partial t^2}=v^2\frac{\partial^2 U}{\partial x^2}+\frac{a^4\gamma\hbar}{M}\frac{\partial S}{\partial x}, \tag{10}$$

$$\left(\frac{\partial^2}{\partial t^2}+\omega^2\right)S=2a\gamma\omega\frac{\partial U}{\partial x}n, \tag{11}$$

$$\frac{\partial n}{\partial t}=-\frac{2a\gamma}{\omega}\frac{\partial U}{\partial x}\frac{\partial S}{\partial t}. \tag{12}$$

The sound velocity v has entered into Eq. (10) via the relation $v=(Ka^2/M)^{1/2}$. Note that Eq. (10) represents a driven mass oscillator, while Eqs. (11) and (12) govern the development of the precessing spin Bloch vector.

To cast Eqs. (10)–(12) into the form favored for Bloch equations, i.e., a set of first-order differential equations, we decompose U and S into left- and right-going waves,

$$U(x,t)=U_Le^{i(kx+\omega t)}+U_Re^{i(kx-\omega t)}+\text{c.c.}, \tag{13}$$

$$S(x,t)=S_Le^{i(kx+\omega t)}+S_Re^{i(kx-\omega t)}+\text{c.c.}, \tag{14}$$

where k is the acoustic wave vector, and $S(x,t)$ is assumed to follow the spatial dependence of $U(x,t)$ on the grounds that the spins do not interact with another. Dropping the fast components, applying the slowly varying envelop approximations $\partial U/\partial t\ll\omega U$, $\partial U/\partial x\ll kU$, and similar approximations for S, and finally incorporating relaxation of the longitudinal and transverse spin components in the standard phenomenological way,[20] we arrive at the set of Bloch equations

$$\frac{\partial U_L}{\partial t}-v\frac{\partial U_L}{\partial x}=\frac{a^4\gamma\hbar}{2Mv}S_L, \tag{15}$$

$$\frac{\partial U_R}{\partial t}+v\frac{\partial U_R}{\partial x}=-\frac{a^4\gamma\hbar}{2Mv}S_R, \tag{16}$$

$$\frac{\partial S_L}{\partial t}=a\gamma kU_Ln-\frac{S_L}{T_2}, \tag{17}$$

$$\frac{\partial S_R}{\partial t}=-a\gamma kU_Rn-\frac{S_R}{T_2}, \tag{18}$$

$$\frac{\partial n}{\partial t}=2a\gamma k(U_R^*S_R+U_RS_R^*-U_L^*S_L-U_LS_L^*)-\frac{(1+2p_0)n+N^*}{T_1}. \tag{19}$$

Note that the precession at the angular frequency ω has been taken out, so that U_L, U_R, S_L, and S_R are amplitude envelopes which, as n, vary slowly in space and time. The last terms in Eqs. (17) and (18) account for dephasing with the time constant T_2, while the last term in Eq. (19) expresses that n strives for thermal equilibrium at the rate $(1+2p_0)/T_1$ in the absence of an acoustic wave. It is a simple task to show, by ignoring the time derivatives in Eqs. (17) and (18) relative to the terms at the right-hand side, that Eqs. (15)–(19) return to rate equations of the form of Eqs. (1)–(3) in case of negligible coherence $(T_2\to0)$.

At this point, we recall that the acoustic wave is observed via its effects on the two-level populations, more specifically N_-/N_0^*. From Eqs. (15)–(19) we see that these effects scale with the unique parameter combination $\kappa\gamma^2N^*$, in which $\kappa=a^5\hbar k/2Mv$ is a well-defined quantity. When comparing Eqs. (15)–(19) with experiment, therefore, independent knowledge of γ and N^* is not required, which substantially reduces the freedom of adjustment. If we wish to derive the initial population density N_0^* from the adjusted $\gamma^2N_0^*$, we have to rely on an estimate for the coupling constant γ. Following Leonardi *et al.*,[21] we find that γ is related to the direct spin-lattice relaxation time T_1 through

$$\frac{1}{T_1}=\frac{\hbar a^2\omega^3}{2\pi NM}\sum_{\sigma}\frac{\gamma_\sigma^2}{v_\sigma^5}. \tag{20}$$

The summation runs over all contributing phonon branches (in ruby primarily the two transverse ones), the argument of the summation has to be averaged over all directions, and N is the number of unit cells per unit of volume. Since no knowledge is available on the angular dependence of γ_σ, we assume γ to be isotropic. A rough, but for our purposes sufficient, estimate for γ is then given by $\gamma^2 \sim \pi NMv^5/\hbar a^2\omega^3 T_1$.

Another point to be addressed is that Eqs. (15)–(19) allow no room for the statistical quantum fluctuations necessary to trigger the phonon avalanche. Population inversion by optical pumping leaves the spin Bloch vector completely upright ($n=N_0^*$, $S_L=S_R=0$), but this is an equilibrium position, albeit an unstable one, under the government of Eqs. (15)–(19). In the theory of optical lasers,[22] a common solution is to tilt the Bloch vector over a small angle ψ_0. An alternative approach, adopted here because it directly connects to the physics, is to let the wave amplitudes U_L and U_R start from a level comparable to their thermal values or, if need arises at higher pumping powers, a somewhat larger level. A single phonon mode of angular frequency $\omega=2\pi\nu$ has a thermal plus zero-point energy content $\hbar\omega(p_0+\frac{1}{2})$, so that the corresponding classical wave has a squared amplitude $U_0^2=\hbar\omega(p_0+\frac{1}{2})/4NM\omega^2$. In the Debye approximation, the number of modes contributing to U_0^2 equals $\rho\Delta\nu=4\pi\nu^2\Delta\nu/v^3$ per acoustic branch. In the case of ruby, $N=1.1\times10^{28}$ m^{-3}, $M=3.6\times10^{-25}$ kg, and $v=6.7$ km/s for transverse phonons along the *a* axis. For frequencies near the present 1.68 cm^{-1}, experiments yielded $\Delta\nu\approx55$ MHz,[11–14] so that $\rho\Delta\nu=1.3\times10^{19}$ m^{-3} for the two transverse acoustic branches added. At 1.4 K, therefore, the acoustic wave amplitudes U_L and U_R are on the order of 1 fm, indeed close to the amplitudes needed in Eqs. (15)–(19).

We finally take acoustic damping into account. Phonon losses include diffuse scattering into the helium bath at the surfaces, ballistic transport to regions beyond the inverted zone, and anharmonic down conversion during flight in the bulk. The latter process is known to be of little significance in ruby.[23] To incorporate phonon relaxation in a simple manner, we therefore introduce an amplitude loss factor R effective at the crystal end faces, i.e., $U_L=-RU_R$ when the wave reflects from the right crystal end, and similarly $U_R=-RU_L$ at the left end. The description is admittedly heuristic, but turns out to be quite satisfactory.

In calculating the evolution of n, as necessary for the comparison with experiment in Sec. V B below, Eqs. (15)–(19) are evaluated numerically. The path covered by the phonons is divided into N_c compartments of length $\Delta x=v\Delta t$, with Δt being a suitable time step. In each compartment, N^*, U_L, and U_R are given appropriate initial values, while S_L and S_R are set to zero. The end compartments also serve to implement the loss factor R in the way discussed above. For the present crystal thickness of 200 μm, $N_c=50$, corresponding to $\Delta t=30$ ns, provides a sufficiently fine maze. The precise procedure of discretization is to some extent outlined in Ref. 24.

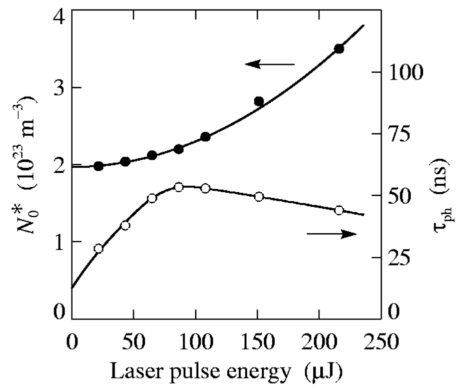

FIG. 3. The parameters N_0^* (filled circles) and τ_{ph} (open circles) fitting the rate Eqs. (1)–(3) to the observed phonon avalanches at various laser pulse energies (dashed curves in Fig. 2). The nonlinear dependence of N_0^* and the inconstancy of τ_{ph} dismiss rate equations as a valid description of the avalanches.

V. COMPARISON WITH EXPERIMENT

A. Rate equations

We first attempt to analyze the data on the avalanche-associated growth of N_- (Fig. 2) on the basis of the incoherent rate Eqs. (1)–(3). Fits of these equations to the temporal development of N_-, separately for each of the laser energies, are represented by the dashed lines in Fig. 2. In these fits, N_0^* and τ_{ph} are the adjustable parameters, while the $\bar{E}(^2E)$ doublet is assumed to be fully inverted immediately after the laser pulse. When we confine ourselves to the dashed lines in Fig. 2, we may all too easily infer that Eqs. (1)–(3) provide an adequate description, leaving improvements to be desired only around the point where the avalanches die out and N_- starts to level off, and, for that matter, at times longer than those included in the figure.

Matters become irreparably inconsistent, however, when we consider the values of the fitted N_0^* and τ_{ph} versus the laser energy (Fig. 3). The rate equations fail to satisfy what is to be expected on physical grounds, viz., that N_0^* increases linearly with the laser energy and that τ_{ph} is constant. The point is that N_- exhibits an S-shaped behavior such as in Fig. 2 for any judicious model of the avalanche, i.e., a slow onset of the phonon density, a subsequent accelerated growth during the avalanche proper, and finally a leveling off when the inversion becomes depleted. For each individual laser energy, therefore, the fit could be made to trace the experiment to a reasonable degree of accuracy, but unphysical values for N_0^* and τ_{ph} were needed to compensate for the deficiencies. In particular, the rate equations do not provide the necessary amplification at low initial inversion, so that the adjusted N_0^* overshoots the true value.

Phonon losses have been included in the rate equations via a term $-(p-p_0)/\tau_{ph}$ representing all kinds of loss

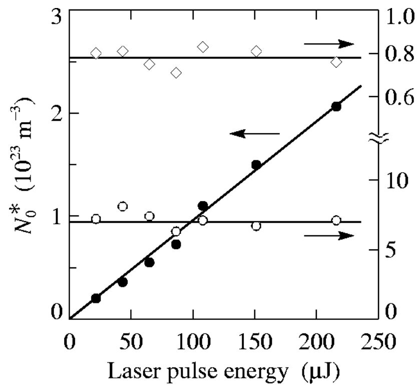

FIG. 4. The parameters N_0^* (closed circles), T_2 (open circles), and R (diamonds) fitting the Bloch Eqs. (15)–(19) to the observed phonon avalanches at various laser pulse energies (solid curves in Fig. 2).

mechanisms. Despite the inconstancy of τ_{ph}, confidence for this comprehensive approach is found in the fact that the distance $v\tau_{ph}\sim 0.3$ mm covered by the phonons in time τ_{ph} is of the order of the size of the inverted zone. As already noted, exceedingly high resonant phonon occupations are reached in the course of the avalanche. We have therefore attempted to improve on Fig. 3 by adding relaxation mechanisms that depend on the phonon density, notably anharmonic up-conversion of the form $-(p-p_0)^2/\tau_a$, which combines two resonant phonons into a single one of double the frequency. Adding this term, which is negligible in the early stages of the avalanche, does however not markedly improve the dependence of N_0^* on the laser energy. We furthermore attempted to improve matters, but again to no avail, by geometry- and position-dependent approaches[3,4] as well as phonon loss by ballistic transport.[23]

B. Bloch equations

We next turn our attention to the Bloch Eqs. (15)–(19), i.e., the coherent equations of motion. Again fits are made to the data on the growth of N_- for each of the laser energies (Fig. 2). As before, the initial condition following pulsed optical pumping is assumed to be complete inversion of $\bar{E}(^2E)$, which in the present context implies a fully upright Bloch vector. The adjustable parameters in Eqs. (15)–(19) are the initial density N_0^* of $\bar{E}(^2E)$, the dephasing time T_2, the phonon loss factor R, and the initial amplitude U_0 of the acoustic waves. The tilting angle ψ_0 was set to zero as its role can be accommodated into U_0. For the present thin sample, N_0^* and U_0 can be taken uniform over the $N_c=50$ compartments introduced for the sake of the numerical evaluation. The results of the fits are shown Fig. 2 as the full lines, and are seen to be remarkably faithful to experiment. As already noted, however, the real test rather lies in the consistency of the parameters from one laser energy to the next.

In Fig. 4 it is observed that T_2 as found from the Bloch equations is independent of the energy of the laser pulse. In fact, the output values for T_2 range between 6 and 8 ns with error margins of about 1 ns, somewhat increasing with deceasing energy on approach of the avalanche threshold. These values are equal to or just above the time associated with the bandwidth of the $E_+\leftrightarrow E_-$ transition, which is inhomogeneously broadened, presumably by orientational wandering of the c axis and other local inhomogeneities.[14] The associated time, in fact, equals $T_2^\dagger=1/\pi\Delta\nu\approx 6$ ns. The similarity indicates that the principal source of dephasing is the frequency spread of the resonant phonons.

Also shown in Fig. 4 are the best values for N_0^* and R. The initial $\bar{E}(^2E)$ population N_0^* now proves to be strictly linear with the laser energy, which self-evidently is an argument of overriding importance in favor of the coherent equations of motion. Independent experiments, such as observation of the luminescent intensity, indeed confirm N_0^* to scale with the laser pulse energy. As concerns the reflection coefficient R, it is, just like T_2 and again according to expectations, independent of the laser power. The output values of the zero-time amplitude of the acoustic wave, U_0, appear to increase monotonically with the laser energy from 0.6 to 2.7 fm. That U_0 grows with the laser energy is however no reason for concern as long as the increase is monotonic and U_0 remains on the order of its thermal value (cf. Sec. IV). The argument here is that the exponentially evolving process of stimulated emission already starts up during the finite time span of the optical pulse, and besides that the origin of the time axis is to some extent arbitrary.

It finally is of interest to convert R to a time that permits comparison with τ_{ph} in the rate equations. In the formalism of the Bloch equations, a damped acoustic wave loses a factor of R in amplitude, and accordingly a factor R^2 in energy, during the time span L/v necessary for flight over the distance L between the crystal faces. The characteristic time for phonon loss therefore amounts to $\tau_e=-L/(2v\ln R)$, with in the present case $L=200$ μm, $v=6.7$ km/s, and $R\approx 0.77$. This leads to $\tau_e\sim 57$ ns, which indeed compares with $\tau_{ph}\sim 50$ ns from the rate equations. The agreement lends further support to the way the coherent model accounts for the phonon decay, viz., by removal at the end faces of the inverted zone.

VI. CONCLUDING REMARKS

We have measured the development of phonon avalanches resonant with the excited $\bar{E}(^2E)$ doublet of Cr^{3+} in dilute ruby. The experimental conditions were specifically adapted to a study of coherence, rather than phonon propagation beyond the excited zone or the effects of the geometry, by reducing the size of the sample. The initial inversion of the doublet is achieved by pulsed optical excitation.

The results have been analyzed in terms of a set of Bloch equations, which are inherently coherent, in comparison with the common approach of incoherent rate equations governing the phonon occupations and the relevant spin populations. Coherence appears to be an essential ingredient in the evolution of the avalanches. Rate equations, on the other hand, may mimic the course of the avalanche provided false values of the parameters are inserted.

The measured dephasing time T_2 compares, within errors, with the time $T_2^{\dagger}$ associated with the width of the one-phonon transition connecting the $\overline{E}(^2E)$ states. As the transition is known to be inhomogeneously broadened,[14] i.e., composed of a conglomerate of one-phonon transitions of different frequencies, T_2 results from the dephasing by the inhomogeneous frequency spread on the one hand and the intrinsic relaxation suffered by the transverse spin components on the other. By analogy with Bloch equations in magnetic resonance,[20] we may therefore write $1/T_2 \sim 1/T_2^{\dagger} + 1/T_2'$, where T_2' is a measure of the loss of coherence by relaxation alone. The present results thus indicate that T_2' significantly exceeds the measured T_2. This taken together with the high amplification the phonons experience by stimulated emission suggests that phonons of a particular frequency maintain a sizable degree of coherence during all of the avalanche.

ACKNOWLEDGMENTS

The authors are indebted to Dr. P. A. van Walree for discussions and to J. G. J. van Lingen for technical assistance. The work was supported by the Netherlands Foundation "Fundamenteel Onderzoek der Materie (FOM)" and the "Nederlandse Organisatie voor Wetenschappelijk Onderzoek (NWO)."

*Electronic address: H.W.deWijn@phys.uu.nl; URL: http://www.phys.uu.nl/~dewijn

[1] W.J. Brya and P.E. Wagner, Phys. Rev. Lett. **14**, 431 (1965); Phys. Rev. **157**, 400 (1967).
[2] J.G.M. van Miltenburg, G.J. Jongerden, J.I. Dijkhuis, and H.W. de Wijn, in *Phonon Scattering in Condensed Matter*, edited by W. Eisenmenger, K. Laßmann, and S. Döttinger, *Springer Series in Solid-State Sciences*, Vol. 51 (Springer-Verlag, Berlin, 1984), p. 130.
[3] P.A. Fokker, J.I. Dijkhuis, and H.W. de Wijn, Phys. Rev. B **55**, 2925 (1997).
[4] P.A. Fokker, R.S. Meltzer, Y.P. Wang, J.I. Dijkhuis, and H.W. de Wijn, Phys. Rev. B **55**, 2934 (1997).
[5] P. A. van Walree, Ph. D. thesis, Utrecht University, 1997; H.W. de Wijn, P.A. van Walree, and A.F.M. Arts, Physica B **263-264**, 30 (1999).
[6] W.E. Bron and W. Grill, Phys. Rev. Lett. **40**, 1459 (1978).
[7] P. Hu, Phys. Rev. Lett. **44**, 417 (1980); M.H.F. Overwijk, J.I. Dijkhuis, and H.W. de Wijn, *ibid.* **65**, 2015 (1990).
[8] D.J. Sox, J.E. Rives, and R.S. Meltzer, Phys. Rev. B **25**, 5064 (1982).
[9] E.M. Ganapolskii and D.N. Makovetskii, Solid State Commun. **15**, 1249 (1974); **90**, 501 (1994).
[10] W.B. Mims and D.R. Taylor, Phys. Rev. Lett. **22**, 1430 (1969); Phys. Rev. B **3**, 2103 (1971).
[11] S. Geschwind, G.E. Devlin, R.L. Cohen, and S.R. Chinn, Phys. Rev. **137**, A1087 (1965).
[12] S. Geschwind, R.J. Collins, and A.L. Schawlow, Phys. Rev. Lett. **3**, 545 (1959).
[13] T. Muramoto, Y. Fukuda, and T. Hashi, J. Phys. Soc. Jpn. **26**, 1551 (1969).
[14] T. Muramoto, J. Phys. Soc. Jpn. **35**, 921 (1973).
[15] M. Blume, R. Orbach, A. Kiel, and S. Geschwind, Phys. Rev. **139**, A314 (1965).
[16] J.I. Dijkhuis, K. Huibregtse, and H.W. de Wijn, Phys. Rev. B **20**, 1835 (1979).
[17] J. de Klerk, Phys. Rev. **139**, A1635 (1965); I.C. Simpson, Philos. Mag. **32**, 293 (1975).
[18] F. Rösch and O. Weis, Z. Phys. B **25**, 101 (1976).
[19] E.H. Jacobsen and K.W.H. Stevens, Phys. Rev. **129**, 2036 (1963).
[20] A. Abragam, *The Principles of Nuclear Magnetism* (Oxford University Press, London, 1961).
[21] C. Leonardi, J.C. MacGillivray, S. Liberman, and M.S. Feld, Phys. Rev. B **11**, 3298 (1973).
[22] F.T. Arecchi and E. Courtens, Phys. Rev. A **2**, 1730 (1970); N.E. Rehler and J.H. Eberly, *ibid.* **3**, 1735 (1971); R. Bonifacio and L.A. Lugiato, *ibid.* **11**, 1507 (1975); **12**, 587 (1975); J.C. MacGillivray and M.S. Feld, *ibid.* **14**, 1169 (1976); M.F.H. Schuurmans, D. Polder, and Q.H.F. Vrehen, J. Opt. Soc. Am. **68**, 699 (1978); Q.H.F. Vrehen and M.F.H. Schuurmans, Phys. Rev. Lett. **42**, 224 (1979).
[23] P.A. van Walree, A.F.M. Arts, and H.W. de Wijn, Phys. Rev. B **64**, 174301 (2001).
[24] J.A. Fleck, Phys. Rev. B **1**, 84 (1969).